On the role of domain aspect ratio in the westward intensification of wind-driven surface ocean circulation

Kaushal Gianchandani[1], Hezi Gildor[1], and Nathan Paldor[1]

[1]Fredy & Nadine Herrmann Institute of Earth Sciences, Hebrew University of Jerusalem, Edmond J. Safra Campus - Givat Ram, Jerusalem, 9190401, Israel

Correspondence: Nathan Paldor (nathan.paldor@mail.huji.ac.il)

Abstract. The two seminal studies on westward intensification, carried out by Stommel and Munk over 70 years ago, are revisited to elucidate the role of the domain aspect ratio (i.e. meridional to zonal extents of the basin) in determining the transport of the western boundary current (WBC). We examine the general mathematical properties of the two models by transforming them to differential problems that contain only two parameters — the domain aspect ratio and the non-dimensional damping (viscous) coefficient. Explicit analytical expressions are obtained from solutions of the non-dimensional vorticity equations and verified by long-time numerical simulations of the corresponding time-dependent equations. The analytical expressions as well as the simulations, imply that in Stommel's model both the domain aspect ratio and the damping parameter contribute equally to the non-dimensional transport of the WBC. On the other hand, in Munk's model the WBC's transport varies linear with the domain aspect ratio, while the damping parameter plays a minor role only. This finding is employed to explain the weak WBC in the South Pacific.

1 Introduction

Perhaps the most striking characteristic of the surface circulation in an ocean basin is the east-west asymmetry: strong and narrow pole-ward directed currents often referred to as the "western boundary currents" (WBCs) flow along the western boundary of the ocean basins while the return equator-ward flow is weak and wide. In the North Atlantic this current is the Gulf Stream, and it was known to oceanographers and explorers for a few centuries — see Stommel (1958) for a historical review. Similar WBCs exist in other basins as well and these include the Kuroshio in the North Pacific and the Brazil current in the South Atlantic. These currents transport large amount of heat from low to high latitudes, thus playing an important role in the climate system. The winds overlying, though, are easterlies along the equator (the Trade winds) and westerlies around 40° N. There are no strong northward winds along the western boundaries of the ocean basins and, as is well understood now, the WBCs are not obviously correlated with the overlying wind patterns. Interestingly, two such WBCs lie in the Pacific viz. the Kuroshio and the East Australian current (EAC). Both the Kuroshio and the EAC are centered close to 26° latitude in their respective

hemispheres and are driven by similar wind stresses and are adjacent to a ~ 2000 km long coastline. Despite these structural similarities, the maximal volumetric transport of the Kuroshio current is 55 Sv (1 Sv $= 10^6$ m^{3}s^{-1}) (Qiu, 2019) whereas that

25 of the EAC is around 30 Sv (Archer et al., 2017). The maximum velocity that EAC attains is also substantially smaller than that of the Kuroshio (Campisi-Pinto et al., 2020).

Henry Stommel, apparently in his first oceanography paper (Stommel, 1948, hereafter referred to as S48) was the first to formulate a simple, yet comprehensive, mathematical model of the WBCs [see e.g. Kunzig (1999)]. S48 is now regarded as a seminal paper in theoretical physical oceanography (e.g. http://empslocal.ex.ac.uk/people/staff/gv219/classics.d/oceanic.html).

30 S48's model probably provides the simplest explanation for the existence of WBCs: in this linear and frictional model on the $\beta-$plane the ocean is taken to be a flat bottom rectangle forced by a cos(latitude)-dependent zonal wind pattern. Walter Munk further extended this work to a different frictional (viscous) parameterization and a more general form of the wind stress (Munk, 1950, hereafter referred to as M50).

In the last 70 years, both models have been modified and extended to further explore the phenomenon of westward intensi-

35 fication in different settings or to evaluate the importance of different specific processes and terms in the governing equations (Munk and Carrier, 1950; Veronis, 1966a, b; Pedlosky, 2013; Vallis, 2017, and references therein).

As in S48 and M50, a large number of these subsequent studies employed the dimensional form of the governing equations which are the time-independent rotating linearized shallow water equations compounded by friction and forcing. These dimensional models include numerous parameters: the zonal and meridional extents of the basin; either the coefficient of linear

40 drag (i.e. the coefficient in the Rayleigh frictional term) or the kinematic eddy viscosity (i.e. the coefficient in parameterization of the viscous term); the amplitude (and possibly meridional structure) of the wind stress; the gradient of Coriolis frequency ($\beta-$effect). On the other hand, a few studies (Welander, 1976; Bye and Veronis, 1979) employed the alternate, concise, approach of non-dimensionalising the governing equation (or the vorticity equation) to investigate the depth averaged wind-driven ocean circulation. The non-dimensional approach not only simplifies the problem by reducing the number of dimensional pa-

45 rameters in the model to fewer non-dimensional ones but also brings out some salient features associated with the problem which are difficult to unveil in the dimensional formulation.

By employing a non-dimensional approach, Welander (1976) successfully identified a zonally uniform regime in both S48's and M50's models of wind-driven ocean circulation and using the same approach, Bye and Veronis (1979) derived a correction to the Sverdrup transport in S48's model. The aforementioned studies highlighted the importance of the ratio between

50 meridional and zonal extents of the basin as one of the two fundamental parameters in both S48's and M50's models. The aim of this study is to further elaborate on the role of the domain aspect ratio (defined here as the ratio between the basin's meridional and zonal extents) in S48's and M50's models of westward intensification. In particular, we examine the role of domain aspect ratio in the transport of the WBC as was first hypothesized by Bye and Veronis (1979) in the context of S48's model, "... the tendency of north-south diffusive processes to be more significant in basins with a large (***small in the present***

55 ***scaling***) aspect ratio makes sense physically and may play a quantitative role in the transport of the western boundary current." We also examine the relevance of our results to the observed difference in strengths of the five WBCs in the world ocean.

The paper is organized as follows. Section 2 outlines our proposed scaling [which is slightly different from the one employed in Welander (1976); Bye and Veronis (1979)] that reduces the number of parameters in the vorticity equations corresponding to S48's and M50's models from five dimensional ones to two non-dimensional ones — one of which is the domain aspect ratio

60 (the other is damping). The solution for the stream function in the two cases is outlined and using this we obtain the expression for the non-dimensional transport of the WBC in both S48's and M50's models. The applicability of the analytical expression of transport for relevant values of the model parameters is validated in Section 3 by simulating the time-dependent equations. We discuss the results and conclude in Section 4. We also note that there were some typos in the expressions of zonal velocity and sea surface height (but not the stream function itself) in S48 and for completeness, we list them in Appendix A. These

65 typos do not change the scientific conclusions drawn in S48.

2 The two-parameter differential problems, their solutions and transport of the WBC

2.1 S48's non-dimensional counterpart

We begin by scaling S48's dimensional vorticity equation for the spatial structure of the stream function as follows: x (the zonal coordinate) on L_x (the basin's zonal extent); y (the meridional coordinate) on L_y (the basin's meridional extent) and

70 ψ (the stream function) on $\gamma \beta L_y^3$ where $\gamma = \tau_0 \left(\dfrac{\pi}{\rho_0 H_0 \beta L_y^2} \right) \left(\dfrac{L_x}{\beta L_y^2} \right)$ is the non-dimensional amplitude of the wind stress (and τ_0 is the wind's dimensional amplitude) with β — the meridional gradient of the Coriolis frequency, H_0 — the depth of the basin and ρ_0 — the water density of the barotropic ocean. With this scaling the non-dimensional form of S48's vorticity equation is:

$$\alpha \nabla^2 \psi + \frac{\partial \psi}{\partial x} = \sin(\pi y) \tag{1}$$

75 $$\alpha = r \left(\frac{L_x}{\beta L_y^2} \right), \quad \nabla^2 = \delta^2 \frac{\partial^2}{\partial x^2} + \frac{\partial^2}{\partial y^2}. \tag{2}$$

Here ∇^2 is the Laplacian, $\delta = \dfrac{L_y}{L_x}$ is the ratio of meridional and zonal extents of the basin (refereed to as the domain aspect ratio) and α is the non-dimensional parameter (referred to as the damping) proportional to r [$\sim 1/10 \, \mathrm{days}^{-1}$] — the Rayleigh friction coefficient. It is evident from (1) and (2) that the two parameters, α and δ, govern the structure of the flow in the basin. The no normal flow conditions at the basin's boundaries mandate that the stream function ψ satisfies the boundary conditions:

80 $\psi(x,0) = \psi(1,y) = \psi(x,1) = \psi(0,y) = 0$.

It should be stressed that due to the different scaling employed in the two works, our α in (1) differs from the corresponding coefficient of damping in Bye and Veronis (1979). Moreover, we use the term domain aspect ratio (δ) to refer to the ratio between meridional to zonal dimensions of the basin which is reciprocal of the domain aspect ratio defined by Bye and Veronis (1979).

85 As has been stated earlier, the non-dimensional formulation lumps the five dimensional parameters in S48's model — zonal and meridional extent of the basin, gradient of Coriolis frequency, wind stress amplitude and Rayleigh friction coefficient — into just two non-dimensional ones: α and δ (that appears in the first term of the Laplacian operator). The interplay between

the three terms in the inhomogeneous partial differential vorticity equation, (1), can be easily interpreted by repeating the procedure employed in S48 to obtain the general form of solutions of (1). An explicit expression for the solution ψ is given by:

90

$$\psi(x,y) = \frac{1}{\alpha \pi^2} \sin(\pi y)(pe^{Ax} + qe^{Bx} - 1) \tag{3}$$

where

$$p = \frac{1 - e^B}{e^A - e^B}$$

$$q = 1 - p$$

95   and

$$A = -\frac{1}{2\alpha\delta^2} + \frac{\pi}{\delta}\sqrt{1 + \frac{1}{4\pi^2\alpha^2\delta^2}},$$

$$B = -\frac{1}{2\alpha\delta^2} - \frac{\pi}{\delta}\sqrt{1 + \frac{1}{4\pi^2\alpha^2\delta^2}}.$$

As is evident from (3), the spatial structure of the stream function is controlled by both α and δ. Fig. 1(a),(c) depict the stream function for two α-regimes of S48's model: (i) weak damping [$\alpha \leq O(1)$] and (ii) strong damping [$\alpha > O(1)$]. For

100   $\alpha \leq O(1)$, the solution ψ given by (3) becomes linear in x and thus can satisfy only one boundary condition out of two. This solution is commonly assumed to approximate the exact solution for ψ in the frictionless interior of the basin while a different approximation applies in the narrow, frictional, boundary layer adjacent to $x = 0$. Fig. 1(a) depicts this narrow boundary layer for $\alpha = 0.1$ where the stream function first decreases fast with x at small x and then increases slowly with x for large x. In the range of $\alpha \geq O(1)$, the solution ψ is symmetric about $x = \frac{1}{2}$ and can satisfy the two boundary conditions,

105   $\psi(0,y) = 0 = \psi(1,y)$. This is demonstrated in the symmetric stream function depicted in Fig. 1(c) for $\alpha = 10$. The explicit expressions of ψ in the two ranges of α are given in the Appendix B.

In the non-dimensional S48's model, the width of the WBC is given by $\epsilon = \alpha\delta^2$ which can be derived from the balance between the Rayleigh friction term and the advection of planetary vorticity in the WBC i.e. $\frac{r}{\beta L_x}$. The definition of the steam function implies that the zonal velocity and the meridional velocity are given by, $u = \frac{\partial \psi}{\partial y}$ and $v = -\delta\frac{\partial \psi}{\partial x}$, respectively. We

110   define the (non-dimensional) transport of the WBC as the product of its width and the mean meridional velocity between the western edge of the basin, $x = 0$, and $x = \epsilon$ evaluated along $y = \frac{1}{2}$ i.e. $Tr = \epsilon\left(\frac{1}{\epsilon}\int\limits_0^\epsilon -\delta\left.\frac{\partial \psi}{\partial x}\right|_{y=\frac{1}{2}} dx\right)$. Though the definition of the WBC's width is somewhat arbitrary for definitiveness we chose it to be ϵ. The integral in the the definition of the transport, Tr, simplifies to the product of the domain aspect ratio and the difference in the values of the stream function evaluated at $x = 0$ and $x = \epsilon$ along $y = \frac{1}{2}$, i.e. $Tr = \delta\left[\psi\left(0,\frac{1}{2}\right) - \psi\left(\epsilon,\frac{1}{2}\right)\right]$. Substituting the boundary condition $\psi\left(0,\frac{1}{2}\right) = 0$ and using the

115   explicit solution (3) yields:

$$Tr = \frac{\delta}{\alpha\pi^2}(1 - pe^{A\epsilon} - qe^{B\epsilon}). \tag{4}$$
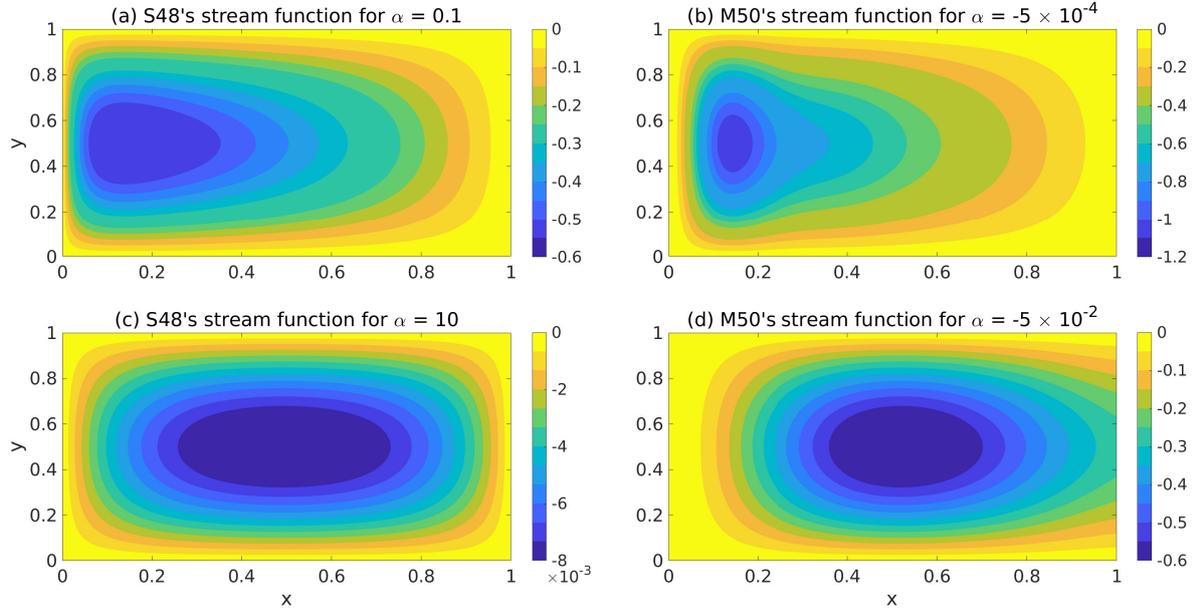
Figure 1. The stream functions in different regimes of the α parameter-space in the two models for $\delta = 2\pi/10$: (a),(b) weak damping [$\alpha \leq O(1)$ in S48's model and $|\alpha| \leq O(10^{-3})$ in M50's model] — there exists a narrow fast flowing current along the western edge of the basin; (c),(d) strong damping [$\alpha > O(1)$ in S48's model and $|\alpha| > O(10^{-3})$ in M50's model] — the stream function is (nearly) symmetric about $x = 0.5$ which indicates that there is no westward intensification.

This expression will be compared below to its counterpart in M50's model and will be compared in section 3 with transports calculated by numerical simulations.

2.2 M50's non-dimensional counterpart

120 The non-dimensional counterpart of M50's vorticity equation, obtained by employing the scaling proposed in this study, is given by:

$$\alpha \nabla^4 \psi + \frac{\partial \psi}{\partial x} = \sin(\pi y) \tag{5}$$

$$\alpha = -\mu \frac{L_x}{\beta L_y^4}, \quad \nabla^4 = \delta^4 \frac{\partial^4}{\partial x^4} + 2\delta^2 \frac{\partial^4}{\partial x^2 \partial y^2} + \frac{\partial}{\partial y^4} \tag{6}$$

where μ ($\sim 10^4 \ \mathrm{m^2 s^{-1}}$) is the (dimensional) horizontal eddy viscosity coefficient. We note that contrary to (2), α in (6) is

125 negative. This dissimilarity arises because, unlike the parametrization in S48, in M50's model the damping is parametrized by a biharmonic function. Also, in addition to stream function vanishing at the edges of the basin another set of boundary condition has to be specified to solve the 4th order equation (5). The additional boundary conditions employed by M50 originate from the inclusion of lateral viscosity which implies that there should be no tangential flow at the basin's edges i.e. $\left. \frac{\partial \psi}{\partial x} \right|_{x=0,1} =$

$\left.\dfrac{\partial \psi}{\partial y}\right|_{y=0,1} = 0$. Following the mathematical steps in M50 yields the following solution of (5):

$$\psi = -\sin(\pi y)\left[1 - x + \frac{1}{\lambda}e^{\lambda(x-1)} - e^{-\lambda(x/2)}\xi(\lambda)\right] \tag{7}$$

where $\lambda = \left(\dfrac{1}{-\alpha\delta^4}\right)^{1/3}$,

and $\xi(\lambda) = \left[\cos\left(\dfrac{\sqrt{3}\lambda x}{2}\right) + \dfrac{1-2/\lambda}{\sqrt{3}}\sin\left(\dfrac{\sqrt{3}\lambda x}{2}\right)\right]$.

Fig. 1(b),(d) depicts the stream function for small and large damping in M50's model. For large damping the stream function shown in Fig. 1(d) is not entirely symmetric about $x = \dfrac{1}{2}$. Also, unlike the behavior of the stream function in S48's model, the stream function in M50's model skews more towards the eastern boundary with the increase in damping. This, less than optimal, behavior of the stream function in M50's model occurs because the stream function does not vanish identically along the eastern boundary and is, instead, a function of α itself (although, this value is not large).

We turn now to the estimation of the WBC's transport in M50's model. As was done in S48's model, this transport is also defined as the product of the boundary layer width ϵ [given by $(-\alpha\delta^4)^{(1/3)} \equiv (|\alpha|\delta^4)^{(1/3)}$ in M50's model] and the mean meridional velocity of the current between $x = 0$ and $x = \epsilon$ along $y = \dfrac{1}{2}$. Following the arguments laid out in the previous section [see the paragraph above (4)] an expression for transport can be obtained by multiplying the domain aspect ratio by the difference of the stream function values between $x = 0$ and $x = \epsilon$ along $y = \dfrac{1}{2}$. Furthermore, substituting the boundary condition $\psi\left(0, \dfrac{1}{2}\right) = 0$ yields $Tr = -\delta\psi\left(\epsilon, \dfrac{1}{2}\right)$. Evaluating ψ in (7) at $\left(\epsilon, \dfrac{1}{2}\right)$ where $\epsilon \ll 1$ yields the following simplified expression for the WBC's transport in M50's model:

$$Tr = \delta\left(1 - e^{(-1/2)}\left[\cos\left(\frac{\sqrt{3}}{2}\right) + \frac{1-2\epsilon}{\sqrt{3}}\sin\left(\frac{\sqrt{3}}{2}\right)\right]\right). \tag{8}$$

In S48's model the transport of the WBC, given by (4), is governed by both damping (α) and domain aspect ratio (δ). This is in agreement with the findings of Bye and Veronis (1979). However, in M50's model the dependence of the WBC's transport on the two parameters is strikingly different. At least to zeroth order, the WBC's transport in M50's model is independent of α and is governed solely by δ. In the next section we validate this claim using numerical simulations and then apply our results to the present-day world ocean.

3 Numerical simulations and application to the world ocean

The numerical simulations described below were carried out using the time-dependent, forced-dissipative, rotating shallow water equation (SWE) dimensional solver that was successfully used in previous studies. The solver employs the finite difference method to solve SWEs on the $\beta-$plane and the simulations are carried out on an Arakawa C grid with leapfrog time difference scheme. Though the solver can include nonlinear terms, these terms were neglected in the present application. The

reader should refer to Gildor et al. (2016) and Shamir et al. (2019) for a more detailed description of the solver. The reader should also note that dimensional variables mentioned in this section are accompanied by an asterisk ($*$).

The simulations presented here were carried out in a barotropic ocean with the same characteristics as in S48 i.e. on an equatorial $\beta-$plane ($f_0 = 0$), forced by a wind stress that varies as $-\tau_0 \cos\left(\dfrac{\pi y^*}{L_y}\right)$. Three of the dimensional parameters remained fixed in all the simulations presented below — the gradient of Coriolis frequency (given by $\beta = 2 \times 10^{-11}$ m^{-1}s^{-1}), the zonal extent of the basin (L_x = 10000 km) and the amplitude of the prescribed forcing ($\tau_0 = 0.2$ Nm^{-2}). The other two dimensional parameters in the two WBC models i.e. the damping coefficients [Rayleigh friction coefficient (r) in S48's model and horizontal eddy viscosity (μ) in M50's model] and the meridional extent of the basin (L_y) are varied to examine the effect of α and δ on the transport. We note that keeping τ_0 fixed and varying L_y will yield different values of γ in the simulation, however, since we scale our ψ^* on $\gamma \beta L_y^3$ and only look at the non-dimensional transport we do not have to account for the effects of changes in γ. The results are consistent with what one would obtain by keeping only β and L_x fixed and varying τ_0 along with the damping coefficients and L_y to keep γ constant. The boundary conditions are: the (dimensional) zonal and meridional velocities vanish along the basin's meridional and zonal boundaries respectively, i.e. $u^*|_{y^*=0,L_y} = v^*|_{x^*=0,L_x} = 0$. The numerical solver is integrated until a steady state is reached. The steady state of the time-dependent simulations is defined as the state at which the dependent variables in the SWEs [dimensional zonal velocity (u^*), meridional velocity (v^*) and sea surface height (η^*)] cease to evolve for sufficiently long time.
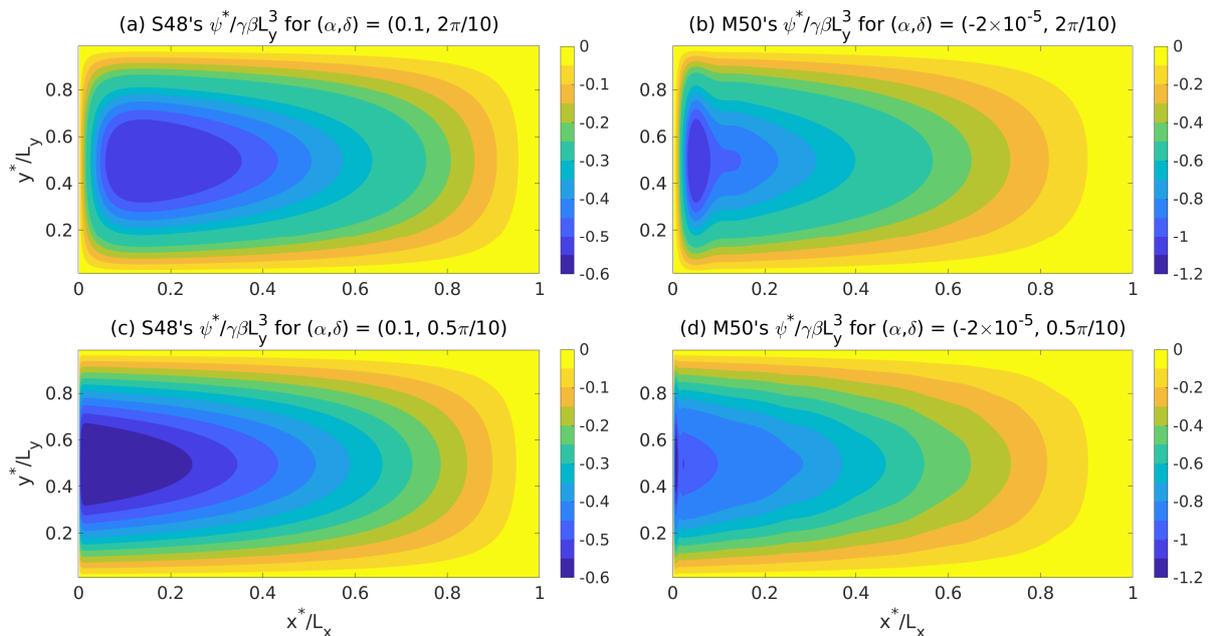
Figure 2. Numerically obtained, non-dimensionalized, stream functions (a) for S48's model — $(\alpha, \delta) = (0.1, 2\pi/10)$ and (b) for M50's model — $(\alpha, \delta) = (-2 \times 10^{-5}, 2\pi/10)$; panels (c),(d) are same as (a),(b) but for $\delta = 0.5\pi/10$. Note that ψ^*, x^* and y^* are scaled on $\gamma \beta L_y^3$, L_x and L_y respectively. Also, the meridional extent of the basin (L_y) in (c),(d) was chosen to be one-fourth of that in (a),(b).
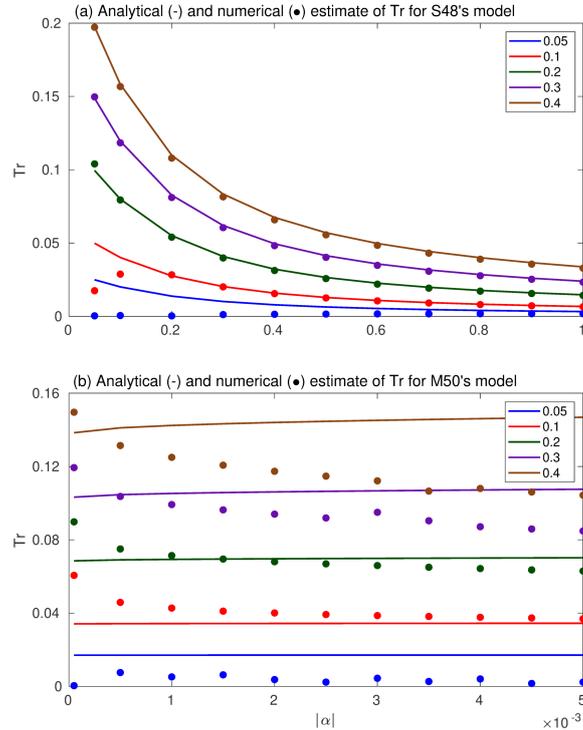
Figure 3. Comparison between analytically (solid lines) and numerically (dots) calculated values of transport (Tr) as a function of $|\alpha|$ for different values of δ in (a) S48's and (b) M50's models.

Fig. 2(a),(c) depicts the numerically obtained, non-dimensional stream function $\left(\psi = \dfrac{\psi^*}{\gamma\beta L_y^3}\right)$ in the steady state for the dimensional parameters as in S48's model (and the corresponding values of α and δ are noted above these panels) while Fig.2(b),(d) depicts the numerically obtained, non-dimensional ψ in the steady state for the parameters relevant to M50's model (and here too the corresponding values of α and δ are noted above these panels). The reader should note that the meridional extent (L_y) of the basin in Fig. 2(a),(b) is $2\pi \times 1000$ km, whereas in Fig. 2(c),(d), $L_y = \pi/2 \times 1000$ km. In all four cases the shape of the stream function is very similar to the steady non-dimensional stream functions shown in Fig. 1(a),(b). We note that for the given values of (α, δ), the ψs obtained from dividing the numerically calculated ψ^*s by the corresponding values of $\gamma\beta L_y^3$ agree very well with the ψ calculated analytically for the same values of (α, δ) using (3) for S48's model and (7) for M50's model.

Fig. 2 depicts that in both S48's and M50's models, for a fixed value of α the width of the WBC increases with δ while the gradient of the stream function (and, in turn, the meridional velocity of the WBC) decreases with it. This indicates that δ exercises a control over the transport of the WBC and hence cannot be ignored.

Fig. 3 compares the analytic and numerically computed values of the non-dimensional transport (Tr) of the WBC in S48's

185 and M50's models as a function of $|\alpha|$ for several values of δ. The solid lines denote the analytic value of Tr obtained from the

expressions given by (4) and (8). The 'numerical transport' of the WBC is obtained by taking the product of δ and $-\dfrac{\psi^*(\epsilon, \frac{1}{2})}{\gamma \beta L_y^3}$.

Here, $\psi^*\left(\epsilon, \dfrac{1}{2}\right)$ is the value of the steady state dimensional stream function at $\left(\epsilon, \dfrac{1}{2}\right)$ obtained from the results of the

numerical simulation for a given set of parameters which correspond to a certain (α, δ); $\epsilon = \alpha \delta^2$ in S48's and $\epsilon = (|\alpha| \delta^4)^{1/3}$

in M50's model.

190 As is evident by Fig. 3 the analytic and numerically calculated non-dimensional transports of the WBC are in agreement for

large values of α in S48's model. However, for small values of both α and δ the numerically calculated transport of the WBC

is smaller than the analytic one. This is because, in S48's model, the gradient of the stream function given by (3) is very large

near the western edge of the basin i.e. the stream lines are 'squished' together, which is not the case in numerical simulations

carried out under the same setting.

195 Fig. 3(b) shows that the analytic transport of the WBC is nearly independent of $|\alpha|$ and is governed primarily by δ. The

numerically calculated transport of the WBC shows a similar behavior, however, there is a notable dependence of the transport

on $|\alpha|$ for small values of the parameter. We also note that there is a discernible difference in the analytically estimated and

numerically calculated values of transport for nearly all values of $(|\alpha|, \delta)$. This is because the value of the stream function

obtained under the assumption $\epsilon \ll 1$ does not hold for large values of $|\alpha|$ and the contribution from the neglected terms

200 becomes significant.

Fig. 4 depicts the non-dimensional transport of the WBC in S48's [panel (a)] and M50's models [panel (b)] as contours on

(α, δ) plane. The contours were obtained by interpolating (using the cubic spline method) between the numerically calculated

values of the WBC's transport as shown in Fig. 3. As is evident from Fig. 4(a), the non-dimensional transport is a function

of both α and δ in S48's model. On the other hand, Fig. 4(b) shows that the transport of the WBC is nearly independent of

205 $|\alpha|$ and is governed primarily by δ (contours nearly parallel the abscissa). The position of the different WBCs in the (α, δ)

parameter space $[(|\alpha|, \delta)$ for M50's model] is marked with different symbols and the errorbars account for the inaccuracies in

the assigned values of the zonal and meridional extents of the basins. The details of how the irregular basins in the world ocean

are approximated with rectangles are discussed in Appendix C. The error in $|\alpha|$ has been omitted from 4(b) because the WBC's

transport in M50's model is nearly independent of $|\alpha|$. Despite the large uncertainty in the damping parameters (relevant in

210 S48's model only) and domain aspect ratios (relevant in both S48's and M50's models) of the five WBCs, the non-dimensional

transport of the East Australian Current (EAC) is distinctly smaller than that of the other WBCs.

4 Summary and Discussions

Since the introduction of the S48's and M50's models about 70 years ago, numerous theoretical and numerical investigations

have been carried out to further explore the characteristics of westward intensification (Munk and Carrier, 1950; Stommel,

215 1958; Hogg and Johns, 1995; Pedlosky, 2013; Vallis, 2017, and references therein). Both S48's and M50's dimensional models
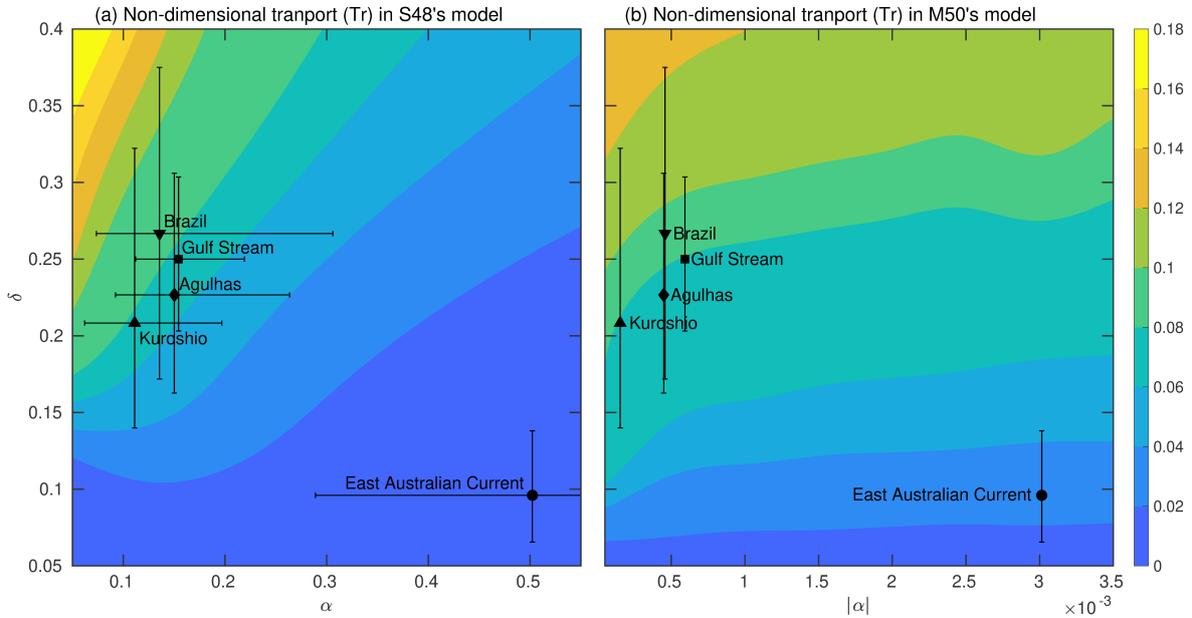
Figure 4. The non-dimensional transport of the western boundary current (WBC) as a function of α and δ in (a) S48's model and (b) M50's model. The different WBCs in the world ocean are depicted with different symbols and the errorbars denote the possible variability of parameters that can occur because of an error in estimating the zonal and meridional extents of the basins that contain the WBC. The error in $|\alpha|$ is not accounted for in (b) because the WBC's transport in M50's model is (nearly) independent of $|\alpha|$. The East Australian Current's (EAC) non-dimensional transport, as calculated from both S48's and M50's models, is less than the other four WBCs. The uncertainty in α for the EAC extends up to 0.9 in S48's model, the contours have been restricted to better resolve the other four boundary currents. The range between which the non-dimensional transport varies is similar in both the models.

clearly bring out the contribution of each source of vorticity: damping, planetary gradient and wind forcing in producing the characteristic east-west asymmetry of the flow in a basin. However, it is difficult to quantify the contribution of each of the five dimensional parameters (L_x, L_y, β, τ_0 and r/μ) to the transport of WBC, using the dimensional models. A better alternative is to combine several dimensional parameters to yield a system with fewer non-dimensional parameters as was employed by, for

220 example, Welander (1976) to identify a zonally uniform regime in ocean circulation and by Bye and Veronis (1979) to identify the correction to the Sverdrup transport in context of S48's original model.

In this article, we address the issue raised by Bye and Veronis (1979) regarding the effect of domain aspect ratio on the WBC's transport by providing explicit expressions of the non-dimensional transport in both S48's and M50's models. These expressions are then benchmarked against numerical simulations of the time dependent, forced-dissipative, rotating shallow

225 water equations. Both the analytic expressions and steady state simulations show that the WBCs' transports depend on both α and δ in S48's model and both the parameters have a similar effect on the transport $\left(Tr \sim \dfrac{\delta}{\alpha}\right)$. In contrast, the transport of the WBC in M50's model is nearly independent of α and is governed primarily by δ ($Tr \sim \delta$).

The non-dimensional formulation presented here does not alter the physical basis of the two models. We emphasize that the dimensional transport (calculated from the product of the non-dimensional transport and $\gamma \beta L_y^3 H_0$) in S48's model varies

230 linearly with the Rayleigh friction coefficient (r) while in M50's model it is nearly independent of the eddy viscosity (μ). On the other hand, in both models the transport varies linearly with the wind-forcing amplitude (τ_0).

The application of our results to present-day ocean attributes the small transport of the EAC compared to the other WBCs to the geometry of the South Pacific ocean. However, factors other than the domain aspect ratio may also be important in determining the transport. For instance, the Brazil current's volumetric transport is low (especially in the northern part) because

235 the current is largely confined to the continental shelf (Stramma et al., 1990). Temperature-driven buoyancy fluxes can also affect the transport of a WBC (Hogg and Gayen, 2020).

It is highly plausible that with a different arrangement of the continents in previous geologic times, the small domain aspect ratio that persisted in the ocean at that time could not support a strong WBC. Thus, the resulting higher pole to equator temperature gradient might have strongly affected the Meridional Overturning Circulation. This hypothesis should be addressed

240 in a future work.

Code availability. The numerical model used in this work can be downloaded from https://github.com/kaushalgianchandani/SWEsolver

Data availability. No data were used or generated in this theoretical research.

Author contributions. All authors contributed equally to this work.

Competing interests. The authors declare no conflict of interest.

245 *Financial support.* This research was supported by the ISF-NSFC joint research program (grant number 2547/17).

The velocity components u and v may be obtained from (8) by simple differentiation of the stream function

$$u = \gamma(b/\pi) \cos(\pi y/b)(pe^{Ax} + qe^{Bx} - 1) \quad \ldots \ldots \ldots \ldots \ldots \quad (21)$$

$$v = -\gamma(b/\pi)^2 \sin(\pi y/b)(pAe^{Ax} + qBe^{Bx}) \quad \ldots \ldots \ldots \ldots \ldots \quad (22)$$

cos(πy/b)

The value of h at any point referred to the value of h at the origin may now be obtained by integration of (1) and (2).

$$h(x,y) = -(F/gD)(e^{Ax}p/A + e^{Bx}q/B) - \cancel{(b/\pi)^2(F/gD)(pAe^{Ax} + qBe^{Bx})[(\cos \pi y/b) - 1]}$$

$$- \left\{ (f\gamma/g)(b/\pi)^2 \sin(\pi y/b) - \cancel{(\partial f/\partial y)(\gamma/g)(b/\pi)^3[\cos(\pi y/b) - 1]} \right\} \left\{ pe^{Ax} + qe^{Bx} - 1 \right\} \quad . \quad (23)$$

+ (∂f/∂y)(γ/g)(b/π)³ cos(πy/b)

Figure A1. Corrections to u and h indicated over excerpts from Stommel (1948).

Appendix A: Typos in Stommel (1948)

There are some typos in the expression for u and η in Stommel (1948). The correct expressions are given as:

$$u = \gamma(b/\pi)\cos(\pi y/b)\left(pe^{Ax} + qe^{Bx} - 1\right) \tag{A1}$$

$$\eta = -(F/gD)\cos(\pi y/b)(e^{Ax}p/A + e^{Bx}q/B)$$

250

$$\qquad -(f\gamma/g)(b/\pi)^2 \sin(\pi y/b)(pe^{Ax} + qBe^{Bx} - 1)$$

$$\qquad +(\partial f/\partial y)(\gamma/g)(b/\pi)^3 \cos(\pi y/b). \tag{A2}$$

For the reader's perusal, the variables in the aforementioned equations are the same as the ones defined in Stommel (1948). Fig. A1 provides excerpts from Stommel (1948) over which, the corrections have been highlighted.

Appendix B: Limiting cases of stream function ψ in S48's model

255   In the limit $\alpha < O(1)$, the solution ψ tends to:

$$\lim_{\alpha < O(1)} \psi(x,y) = \frac{c_1}{\alpha\pi^2}\sin(\pi y)(x) \tag{B1}$$

where $c_1 = \lim\limits_{\alpha < O(1)} A$ is a number $\ll 1$. On the other hand, in the limit of $\alpha > O(1)$, the solution ψ becomes:

$$\lim_{\alpha > O(1)} \psi(x,y) = \frac{1}{\alpha\pi^2}\sin(\pi y)[p(e^{c_2 x} + e^{c_2(1-x)}) - 1] \tag{B2}$$

where $c_2 = \lim_{\alpha > O(1)} A = \frac{\pi}{\delta}$ and $p = \frac{e^{c_2} - 1}{e^{2c_2} - 1}$. The function $\lim_{\alpha > O(1)} \psi(x, y)$ is symmetric about $x = \frac{1}{2}$.

Appendix C: Zonal and meridional extents of the five western boundary currents in present-day world ocean

To determine the zonal and meridional extents of a basin containing a WBC, we identified the mean initiation and termination latitudes of each WBC based on the available literature. The Gulf Stream begins at the tip of Florida ($\sim 25°$ N) and runs upto $\sim 38°$ N where it breaks of into hot and cold rings (Hogg and Johns, 1995). The Kuroshio originates from the bifurcation of North Equatorial current at 12 - 13° N, although this bifurcation point can vary between 10 - 15° N (Qiu and Lukas, 1996); it separates from the Japan coast at 35° N as a meandering current colloquially known as the Kuroshio extension which stretches as far as $\sim 38°$ N (Kida et al., 2016). The East Madagascar-Agulhas current, in the South Indian ocean, runs from 20° S to 40° S (Lutjeharms et al., 1981; Gordon, 1985; Lutjeharms, 2006) — however the current retroflects between 38° S to 40° S (Quartly and Srokosz, 1993). Moreover, the African continental landmass ends close to 35° S. The Brazil current begins between 10° S and 12° S (Peterson and Stramma, 1991; Stramma et al., 1990) but the intense current attains its intense speed characteristic of a WBC only when it crosses the Vitoria-Trindade Ridge at 20.5° S (Evans et al., 1983). This current separates from the coastline at a mean value of 36° S $\pm$ 1.1° (Olson et al., 1988). The last of the five WBCs in the world ocean is the East Australian Current (EAC) that extends from 18° S to around 35° S (Boland and Church, 1981; Ridgway and Godfrey, 1994) but a characteristic southward flow is evident only when EAC crosses 22° S (Ridgway and Dunn, 2003); the current usually separates from the coast at 33° S (Archer et al., 2017).

We define the meridional extent (L_y) is defined as the distance between the initiation and termination latitudes of the WBC. On the other hand, to determine the zonal extent (L_x) we calculated the distances between the land masses at both the initiation latitude and termination latitude. The average of the two distances is defined as the typical L_x for any given WBC. For instance, the approximate initiation and termination coordinates for the Kuroshio are 13° N, 125° E and 35° N, 140 E respectively, which yields $L_y \approx 2500$ km. The distances to the opposite landmass, the North American continent (which forms the eastern boundary of the basin) as calculated from the initiation coordinate and termination coordinate are ~ 9000 km and ~ 15000 km respectively. Thus, the typical zonal extent of the basin is assumed to be 12000 km.

The mean dimensions L_x and L_y for all the five WBCs in the world ocean are given by Table 1. The 'error' in L_y accounts for the variation between different references of the initiation and termination latitudes and the error in L_x is the deviation of the measured zonal distances along initiation and termination latitude from the mean value. Based on these values of L_x and L_y a range of parameters damping (α) and domain aspect ratio (δ) corresponding to every WBC was estimated and these values of α and δ were employed it to distinguish between the five WBCs. Typical values of L_x and L_y for the ocean basins that contain the WBCs were also estimated using the mean streamlines in the ocean as calculated by Maximenko et al. (2009) — these values were well within the range cited in Table C1.

Table C1. Dimensions of the gyres that contain the five western boundary currents in the present-day world ocean.

Current	Western edge of the basin		Eastern edge of the basin		Basin's dimensions	
	Initiation	Termination	Initiation	Termination	Zonal (L_x)	Meridional (L_y)
Gulf Stream	25° N 80° W	38° N 75° W	25° N 16° W	38° N 10° W	6000 ± 400 km	1500 ± 200 km
Kuroshio	13° N 125° E	35° N 140° E	13° N 92° W	35° N 121° W	12000 ± 3000 km	2500 ± 400 km
Madagascar-Agulhas	20° S 50° E	35° S 20° E	20° S 116° E	35° S 116° E	7500 ± 800 km	1700 ± 350 km
Brazil	21° S 40° W	35° S 54° W	21° S 13° E	35° S 19° E	6000 ± 400 km	1600 ± 500 km
East Australian	22° S 150° E	33° S 152° E	22° S 70° W	33° S 72° W	12500 ± 2000 km	1200 ± 250 km

References

290   Archer, M. R., Roughan, M., Keating, S. R., and Schaeffer, A.: On the Variability of the East Australian Current: Jet Structure, Meandering, and Influence on Shelf Circulation, Journal of Geophysical Research: Oceans, 122, 8464–8481, 2017.

Boland, F. and Church, J.: The East Australian current 1978, Deep Sea Research Part A. Oceanographic Research Papers, 28, 937–957, 1981.

Bye, J. and Veronis, G.: A Correction to the Sverdrup Transport, Journal of Physical Oceanography, 9, 649–651, 1979.

Campisi-Pinto, S., Gianchandani, K., and Ashkenazy, Y.: Statistical tests for the distribution of surface wind and current speeds across the
295   globe, Renewable Energy, 149, 861 – 876, 2020.

Evans, D. L., Signorini, S. R., and Miranda, L. B.: A Note on the Transport of the Brazil Current, Journal of Physical Oceanography, 13, 1732–1738, 1983.

Gildor, H., Paldor, N., and Ben-Shushan, S.: Numerical simulation of harmonic, and trapped, Rossby waves in a channel on the midlatitude β-plane, Quarterly Journal of the Royal Meteorological Society, 142, 2292–2299, 2016.

300   Gordon, A. L.: Indian-Atlantic Transfer of Thermocline Water at the Agulhas Retroflection, Science, 227, 1030–1033, 1985.

Hogg, A. M. C. and Gayen, B.: Ocean Gyres Driven by Surface Buoyancy Forcing, Geophysical Research Letters, p. e2020GL088539, 2020.

Hogg, N. G. and Johns, W. E.: Western boundary currents, Reviews of Geophysics, 33, 1311–1334, 1995.

Kida, S., Mitsudera, H., Aoki, S., Guo, X., Ito, S.-i., Kobashi, F., Komori, N., Kubokawa, A., Miyama, T., Morie, R., et al.: Oceanic fronts and jets around Japan: a review, in: "Hot Spots" in the Climate System, pp. 1–30, Springer, 2016.

305   Kunzig, R.: The Restless Sea: Exploring the World Beneath the Waves, WW Norton & Company, 1999.

Lutjeharms, J., Bang, N., and Duncan, C.: Characteristics of the currents east and south of Madagascar, Deep Sea Research Part A. Oceanographic Research Papers, 28, 879–899, 1981.

Lutjeharms, J. R.: The Agulhas Current, vol. 5, Springer, 2006.

Maximenko, N., Niiler, P., Centurioni, L., Rio, M.-H., Melnichenko, O., Chambers, D., Zlotnicki, V., and Galperin, B.: Mean Dynamic
310   Topography of the Ocean Derived from Satellite and Drifting Buoy Data Using Three Different Techniques*, Journal of Atmospheric and Oceanic Technology, 26, 1910–1919, 2009.

Munk, W. H.: On the wind-driven ocean circulation, Journal of Meteorology, 7, 80–93, 1950.

Munk, W. H. and Carrier, G. F.: The Wind-driven Circulation in Ocean Basins of Various Shapes, Tellus, 2, 158–167, 1950.

Olson, D. B., Podesta, G. P., Evans, R. H., and Brown, O. B.: Temporal variations in the separation of Brazil and Malvinas Currents, Deep Sea Research Part A. Oceanographic Research Papers, 35, 1971–1990, 1988.

Pedlosky, J.: Geophysical Fluid Dynamics, Springer Science & Business Media, 2013.

Peterson, R. G. and Stramma, L.: Upper-level circulation in the South Atlantic Ocean, Progress in Oceanography, 26, 1–73, 1991.

Qiu, B.: Kuroshio and Oyashio Currents☆, in: Encyclopedia of Ocean Sciences (Third Edition), edited by Cochran, J. K., Bokuniewicz, H. J., and Yager, P. L., pp. 384 – 394, Academic Press, Oxford, third edition edn., 2019.

Qiu, B. and Lukas, R.: Seasonal and interannual variability of the North Equatorial Current, the Mindanao Current, and the Kuroshio along the Pacific western boundary, Journal of Geophysical Research: Oceans, 101, 12 315–12 330, 1996.

Quartly, G. and Srokosz, M.: Seasonal Variations in the Region of the Agulhas Retroflection: Studies with Geosat and FRAM, Journal of Physical Oceanography, 23, 2107–2124, 1993.

Ridgway, K. and Dunn, J.: Mesoscale structure of the mean East Australian Current System and its relationship with topography, Progress in Oceanography, 56, 189–222, 2003.

Ridgway, K. and Godfrey, J.: Mass and heat budgets in the East Australian current: A direct approach, Journal of Geophysical Research: Oceans, 99, 3231–3248, 1994.

Shamir, O., Yacoby, I., Ziskin Ziv, S., and Paldor, N.: The Matsuno baroclinic wave test case, Geoscientific Model Development, 12, 2019.

Stommel, H.: The westward intensification of wind-driven ocean currents, Eos, Transactions American Geophysical Union, 29, 202–206, 1948.

Stommel, H.: The Gulf Stream: A Physical and Dynamical Description, Univ of California Press, 1958.

Stramma, L., Ikeda, Y., and Peterson, R. G.: Geostrophic transport in the Brazil Current region north of 20° S, Deep Sea Research Part A. Oceanographic Research Papers, 37, 1875–1886, 1990.

Vallis, G. K.: Atmospheric and Oceanic Fluid Dynamics: Fundamentals and Large-scale Circulation, Cambridge University Press, 2017.

Veronis, G.: Wind-driven ocean circulation—Part 1. Linear theory and perturbation analysis, in: Deep Sea Research and Oceanographic Abstracts, vol. 13, pp. 17–29, Elsevier, 1966a.

Veronis, G.: Wind-driven ocean circulation—Part 2. Numerical solutions of the non-linear problem, in: Deep Sea Research and Oceanographic Abstracts, vol. 13, pp. 31–55, Elsevier, 1966b.

Welander, P.: A Zonally Uniform Regime in the Oceanic Circulation, Journal of Physical Oceanography, 6, 121–124, 1976.